ACCSCIENCE PUBLISHING

Innovative Medicines & Omics

ORIGINAL RESEARCH ARTICLE

Synthesis, spectroscopic characterization, density functional theory analysis, and molecular docking studies of diorganotin (IV) complexes with sterically congested ligands

Shama Chauhan[1], Harlal Singh[2], Venkatanarayana Pappula[3] and Rupa Madyal[1]*

[1]Department of Chemistry, National Defence Academy, Pune, Maharashtra, India

[2]Department of Chemistry, School of Liberal Arts and Sciences, Mody University of Science and Technology, Lakshmangarh, Rajasthan, India

[3]School of Sciences, Woxsen University, Hyderabad, Telangana, India

Abstract

Diorganotin (IV) complexes have attracted considerable attention due to their diverse structural features and promising biological properties. The investigation into diorganotin (IV) compounds as potential antimicrobial agents is an active and captivating area of research, particularly emphasizing the synthesis and characterization of diorganotin (IV) complexes with bioactive and sterically hindered ligands. In this study, novel diorganotin (IV) azomethine chelates were synthesized from sterically hindered 4-(2′-mercapto-phenyl-iminoaryl/alkyl)-2,4-dihydro-5-methyl-2-phenyl-3H-pyrazol-3-ones, characterized, and evaluated for their antimicrobial potential. These complexes were obtained by reacting dimethyltin dichloride with the corresponding disodium salts in benzene and characterized through infrared, ^{1}H, ^{13}C, and ^{119}Sn nuclear magnetic resonance spectroscopy, along with molecular weight determination. Structural optimization and electronic property analyses were performed using density functional theory (DFT) at the B3LYP/LanL2DZ level. Conceptual DFT descriptors indicated subtle variations in reactivity, with Chelate-4 exhibiting the highest softness and the lowest energy gap, suggesting enhanced electron-accepting capability. Molecular docking studies were conducted on the ligand moieties (L-1 to L-4) against proteins from Gram-positive and Gram-negative bacteria using cephalosporin and sulfamethoxazole as reference drugs. Ligand L-4 displayed superior binding affinities across all targets, aligning with its DFT-predicted reactivity. Absorption, distribution, metabolism, and excretion analysis revealed that while L-1 and L-2 showed favorable drug-likeness and oral bioavailability, L-4 demonstrated higher lipophilicity and possible metabolic concerns despite its potent antibacterial potential.

Keywords: Dimethyltin dichloride; Infrared; Nuclear magnetic resonance; Azomethines; ADME; Molecular docking; Density functional theory

***Corresponding author:**
Rupa Madyal
(chemasstprof2nda.ids@gov.in)

Citation: Chauhan S, Singh H, Pappula V, Madyal R. Synthesis, spectroscopic characterization, density functional theory analysis, and molecular docking studies of diorganotin (IV) complexes with sterically congested ligands. *Innov Med Omics*. 2025;2(3):68-82. doi: 10.36922/IMO025140019

Received: April 3, 2025

Revised: July 7, 2025

Accepted: July 10, 2025

Published online: July 31, 2025

1. Introduction

There has been an increasing interest in research in the field of organotin (IV) chemistry due to the ease with which modern physical techniques can be applied to organotin compounds, as well as their fascinating structural and toxicological properties.[1] Numerous studies have been conducted on the synthesis of organotin derivatives, which often include ligands such as alkyl, carboxylates, xanthates, Schiff bases, phenanthroline, and dipeptides.[2-18] Many of these derivatives have also been investigated for their antimicrobial, antitumor, and anti-inflammatory properties.[4,9-18] Organotin-phenanthroline complexes have demonstrated promising biological activities, including antimicrobial and anticancer properties, as the metal-nitrogen coordination enhances the stability and reactivity of the complex.

Medicinal chemistry and drug design have advanced significantly through the use of computational methods for the virtual screening of molecules as potential drug candidates, as they reduce both costs and time. Molecular docking and density functional theory (DFT) methods are efficient computational approaches widely used in the drug development process.[19,20] Molecular docking assesses the binding compatibility of molecules (ligands) with their target (receptor), while DFT calculations enable the evaluation of several electronic descriptors that characterize molecular reactivity.[21] These include measurements of electron distribution properties (electronegativity), resistance to electronic changes (chemical hardness), electron flow tendencies (chemical potential), and electron-accepting capacity (electrophilicity index). Numerous studies have employed two key computational approaches, namely DFT and molecular docking, to unveil potential biomedical applications of tin (Sn) complexes.[14-18] These significant applications of organic derivatives of Sn complexes have stimulated further studies in this field. However, neither experimental nor theoretical studies of pentacoordinated diorganotin (IV) azomethine chelates are available. Our work provides new experimental and theoretical data that could reveal unique structural features and reactivity profiles. These data provide a foundation for future studies on similar compounds.

In this paper, we report the preparation, spectral elucidation, structural aspects, molecular docking, and DFT study of several organotin complexes resulting from sterically overcrowded 4-(2'mercapto-phenyl-iminoaroyl/alkyl)-2,4-dihydro-5-methyl-2-phenyl-3H-pyrazol-3-ones. It is of interest to investigate the interaction of these sterically congested ligands to examine their microbicidal activity. Therefore, molecular docking was used to determine the binding affinity of these ligands with the bacterial protein. In addition, absorption, distribution, metabolism, and excretion (ADME) prediction analysis was performed for ligands L-1 to L-4 to further assess their drug-likeness potential.

2. Methodology

2.1. Experimental methodology

The reaction was carried out under anhydrous conditions, and the solvent was dried using standard methods. The molecular weight (MW) was determined osmotically on a vapor pressure osmometer (Model K-7000, Knauer, Germany) in chloroform ($CHCl_3$) solution at 45°C. Sulfur was estimated using the Messenger's method.[22] Dimethyltin dichloride and dibutyltin dichloride were distilled before use. The synthesized organotin (IV) chelates, resulting from Schiff bases, follow a similar procedure. Nuclear magnetic resonance (NMR) spectra (^1H and ^{13}C) were recorded on an NMR spectrometer (DELTA-2, JEOL, Japan), using tetramethylsilane (TMS) as the internal reference. With the help of potassium bromide (KBr) pellets, the infrared (IR) spectrum was recorded from 4,000 to 400 cm^{-1} using a spectrophotometer (SP-2, PerkinElmer, USA).

For the synthesis of 4-(2'-mercapto-phenyl-iminobenzoyl)-2,4-dihydro-5-methyl-2-phenyl-3H-pyrazol-3-onato dimethyltin (IV), sodium metal weighing 0.143 g (6.2 mmol) was dissolved in about 10.0 mL of methanol. A benzene solution of 4-(2'-mercapto-phenyl-iminobenzoyl)-2,4-dihydro-5-methyl-2-phenyl-3H-pyrazol-3-ones (5 mL, 0.62 M) was then added dropwise, followed by a 5-h reflux. A benzene solution of dimethyltin dichloride (5 mL, 0.62 M) was then added dropwise, and the reaction mixture was refluxed for about 5 h. The reaction mixture was then allowed to cool, and the resultant sodium chloride (NaCl) precipitate was filtered off. The precipitated NaCl was decanted, and the fraction of volatile matter was removed. White to dark brown-colored solid products were obtained. The chelated products were soluble in common organic solvents, such as benzene and chloroform, but insoluble in petroleum ether and n-hexane. The complex compounds were subjected to recrystallization from a chloroform/petroleum ether mixture. Osmometric MW analysis in chloroform solution at 45°C showed that the substances were monomeric. Further characterization of the complexes was carried out using spectral techniques (^1H, ^{13}C, ^{119}Sn NMR, and IR).

Similarly, the remaining three diorganotin (IV) complexes were synthesized through the reaction of 4-(2'-mercapto-phenyl-iminobenzoyl)-2,4-dihydro-5-methyl-2-phenyl-3H-pyrazol-3-one with dimethyltin dichloride in the presence of sodium methoxide. The formation of the desired chelates was confirmed based

on their physical properties, percentage yields, MW estimations, and elemental analyses.

2.2. Computational methods

The geometrical parameters of the ligands (L-1, L-2, L-3, and L-4) and their corresponding Sn complexes, referred to as chelates (Chelate-1, Chelate-2, Chelate-3, and Chelate-4), were optimized using the DFT/B3LYP method with the LanL2DZ basis set, performed through the Gaussian 03W software package (Revision 03, Gaussian, Inc., USA).[23] No initial symmetry constraints were applied during the optimization process. The normal frequencies for the optimized structures were calculated through Hessian analysis.

2.2.1. Molecular docking

Molecular docking simulations predicted ligand-protein interactions and binding energies for Sn complexes, investigating their antibacterial activity. Two protein targets, one from Gram-positive (*Staphylococcus aureus*) and one from Gram-negative (*Escherichia coli*) bacteria, were selected to represent different antibacterial mechanisms. DFT-optimized ligands (L-1 to L-4), along with control molecules (cephalosporin and sulfamethoxazole), were analyzed to provide a comparative assessment. Docking was performed using the standard operating procedure and default settings of AutoDock (Version 4.2.6, Scripps Research, USA), which employs an empirical free energy function. All water molecules were removed from the bacterial protein structures (protein database codes: 5TW8, 6NTW, 1AD4, and 5V7A) during preparation in AutoDock tools, and only polar hydrogens were added to the proteins. The different ligand conformers were generated using a Lamarckian genetic algorithm with an adaptive search method in AutoDock, and the interactions between the ligands and the target receptor were analyzed using Discovery Studio Visualizer (Discovery Studio® 24.1, BIOVIA, USA).

2.2.2. Ligands, control ligands, and protein preparation

DFT-optimized structures of ligands (chelates devoid of central metal ion, i.e., Ti^{2+} ion), named as L-1, L-2, L-3, and L-4, were further subjected to molecular simulation to inspect the antibacterial activity of ligands. The chemical structures of control molecules, cephalosporin (CID: 25058126), and sulfamethoxazole (CID: 5329), were retrieved from the PubChem database (https://pubchem.ncbi.nlm.nih.gov/).

Bacterial targets, including dihydropteroate synthase (1AD4 and 5V7A)[24,25] and transpeptidase (5TW8 and 6NTW),[26,27] were chosen to represent well-known bacterial targets of antibiotics and are summarized in Table 1. These proteins are also relevant for exploring potential avenues for minimizing microbial resistance to antimicrobial agents.[28] Cephalosporins act as bacterial transpeptidase inhibitors,[29,30] while sulfamethoxazole targets the bacterial enzyme dihydropteroate synthase by acting as a competitive inhibitor.[31,32] Accordingly, molecular docking of cephalosporins was performed with target proteins 5TW8 and 6NTW, and sulfamethoxazole was docked with 1AD4 and 5V7A. The docking analysis utilized automated docking procedures with Gasteiger charge assignments applied to all molecular structures. A visualization software package enabled detailed examination of the interactions between the ligands and their protein targets. The docking region was defined by a cubic grid with dimensions of 60 units in each direction and a grid spacing of 0.375 Å, centered on the protein's active site (Table 1).[28]

3. Results and discussion

Dimethyltin dichloride reacts with the Schiff bases in its disodium salt form derived from substituted pyrazolones in an equal molar ratio in a solution of benzene (Figure 1). The formation of the desired chelates was confirmed through the analysis of physical properties, percentage yields, MW estimations, and elemental content. A summary of these data is presented in Table 2. Melting points of the complexes ranged from 108°C to 130°C, indicating moderately high thermal stability, which is characteristic of organotin (IV) complexes. Yields varied from 68% to 79%, with Chelate-4 showing the highest yield, suggesting efficient complexation under the adopted reaction conditions. The experimental values of Sn% and sulfur (S)% were in good agreement with the calculated values, further confirming the proposed compositions.

3.1. Spectroscopic studies

3.1.1. IR spectra

The IR spectra of the complexes, recorded using KBr pellets in the 4,000 – 400 cm^{-1} range, showed significant changes upon coordination. The broad band observed between 3,440 and 3,295 cm^{-1} in the free ligand, attributed

Table 1. Molecular docking targets of selective bacteria with their protein database ID and coordinates

Bacteria target	Gram	Protein database ID	Coordinate		
			X	Y	Z
Transpeptidase	Gram+ve	5TW8	21.390	−62.210	36.200
	Gram−ve	6NTW	21.480	−32.370	42.150
Dihydropteroate synthase	Gram+ve	1AD4	33.106	8.125	41.463
	Gram−ve	5V7A	−17.836	7.522	103.740

Table 2. Synthetic, physical, and elemental data of the diorganotin (IV) complexes, with calculated values given in parentheses

No.	Compound	Melting point (°C)	Yield (%)	Molecular weight (g/mol) analyzed (calculated)	Sodium chloride filtered (g) (calculated)	Elemental analysis (%) (calculated)	
						Tin (Sn)	Sulfur (S)
1	Chelate-1	110	78	470.00 (470.18)	0.19 (0.20)	25.18 (25.24)	6.75 (6.82)
2	Chelate-2	130	68	482.00 (484.18)	0.22 (0.24)	24.48 (24.51)	6.58 (6.62)
3	Chelate-3	108	72	530.00 (532.23)	0.35 (0.36)	22.38 (22.30)	5.95 (6.02)
4	Chelate-4	112	79	570.00 (566.67)	0.38 (0.39)	20.86 (20.95)	5.63 (5.66)

to –OH and > NH groups, disappeared in the spectra of the corresponding organotin (IV) chelates. In addition, the appearance of a new band in the 1,625 – 1,645 cm^{-1} range indicates the presence of the stretching frequency (ν) > C=N–group.[33] In addition, a band detected in the range of 660 – 625 cm^{-1} is assigned to ν S–oxygen (O)[13] (asymmetric ν). The presence of the Sn-S bond is supported by the appearance of the ν Sn-S[6,7] absorption band in the region 422 – 402 cm^{-1}. A weak absorption band of low intensity in the region 456 – 425 cm^{-1} is associated with Sn–N bonds.[2] The presence of these bands indicates the formation of Sn–O, Sn–S, and Sn–N bonds, supporting the bifunctional tridentate coordination mode of the Schiff bases in the organotin (IV) chelates.

3.1.2. ^{1}H NMR

The ^{1}H NMR spectra were recorded in $CDCl_3$/DMSO-d_6 using TMS as the internal standard. A summary of the chemical shifts observed is presented in Table 3. The broad signal at δ 4.96 ppm, attributed to >NH/–SH protons in the Schiff bases,[3] is absent in the spectra of the organotin (IV) chelates, indicating deprotonation of these functional groups. The signal for ring methyl protons is observed at δ 1.69 – 2.46 ppm as a singlet.

No significant shifts were detected in their position compared with their positions in parent ligands. In Chelate-1, the signal for the terminal proton appears at δ 2.42 ppm as a broad singlet. In contrast, for Chelate-2 and Chelate-4, the terminal protons resonate as a quartet at δ 2.78 – 2.86 ppm, corresponding to > CH_2 protons, and as a triplet at δ 1.05 – 1.11 ppm, attributed to –CH_3 protons. The methyl protons bonded to the Sn atom are observed as a singlet in the range of δ 0.83 – 1.45 ppm, while the butyl protons attached to the Sn atom exhibit a complex pattern between δ 0.61 and 2.48 ppm. The value of Sn-hydrogen (H) J coupling, ^{2}J(Sn-H) for Chelate-1 was found to be 100.59 Hz.[34] The proton signals from the phenyl ring (C_6H_5/C_6H_4), as well as those from the thiophenol ring, are merged, and the aromatic protons appear as a complex pattern in the range δ 6.38 – 8.33 ppm. Thus, ^{1}H NMR spectral studies also support the bifunctional tridentate nature of the ligand.

Table 3. The ^{1}H nuclear magnetic resonance spectral data of organotin (IV) complexes (in δ ppm)

Chelate	Ring methyl	Ring/terminal C_6H_5/C_6H_4Cl thiophenol ring	Terminal protons		Sn-R	^{2}J(Sn-H)
			>CH_2	–CH_3		
Chelate-1	2.42 bs	6.54 – 7.99 m	-	2.42 bs	0.83 bs	100.59 Hz
Chelate-2	2.45 s	6.90 – 8.28 m	2.86 q	1.05 t	1.05 bs	-
Chelate-3	1.88 s	6.84 – 8.24 m	-	-	1.08 s	-
Chelate-4	1.97 s	7.26 – 8.22 m	-	-	1.45 s	-

Abbreviations: bs: Broad singlet; q: Quartet; R: functional group; s: Singlet; t: Triplet.

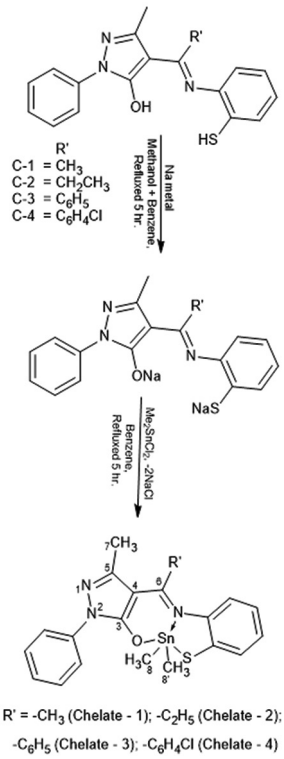

Figure 1. Synthetic pathway for the preparation of diorganotin (IV) chelates (Chelate-1 to Chelate-4)

3.1.3. ^{13}C NMR

The ^{13}C NMR spectra of the complexes were obtained in chloroform using TMS as the reference standard. The

chemical shift values are summarized in Table 4. Comparing the position of the C_6 carbon signal in organotin (IV) chelates with its position in the Schiff bases,[4] an up-field shift is observed. Further, a downfield shift is observed for the C_3 and C_4 carbon signals. The signal for the ring methyl carbon resonates in the range of δ 15.20 – 17.51 ppm. In Chelate-2 and Chelate-4, the terminal carbon signals are observed at δ 9.17 – 11.87 ppm for the $-CH_2$ group and δ 32.84 – 33.32 ppm for the $-CH_3$ group. The carbon atom of the methyl group bonded to the Sn atom shows a signal in the range of δ 7.87 – 8.87 ppm. The butyl carbon signals attached to the central Sn atom are observed at δ 13.52 – 29.30 ppm. The terminal C_6H_5/C_6H_4Cl, ring phenyl, and thiophenol ring carbon atoms are observed at δ 115.09 – 149.09 ppm. Therefore, ^{13}C NMR spectral evidence is also in agreement with IR and ^1H NMR spectral studies.

3.1.4. ^{119}Sn NMR spectra

The ^{119}Sn NMR spectra of these chelates were recorded in chloroform, with tetramethyltin used as an external reference. ^{119}Sn NMR spectroscopy is one of the specialized techniques[34] that provide necessary information on the structures of organotin compounds. Values of chemical shift observed in the case of phenyl and chlorophenyl substituents are δ −116.2 and −105.9, respectively, whereas for ethyl group is observed at δ −143.6.

Table 4. The ^{13}C nuclear magnetic resonance spectral data of organotin (IV) complexes (in δ ppm)

Parameter	Chelate 1	Chelate 2	Chelate 3	Chelate 4
C_3 (C=O)	161.68	160.5	162.2	162.09
C_4 (C=N)	104.56	103.85	104.4	104.29
C_5 (C=N–N)	138.22	138.8	138.58	138.1
C_6 (C=NR')	192.68	197.7	191.9	190.65
C_7 (CH_3 on pyrazolone)	17.34	15.2	16.1	16.31
$-CH_2$ (R' in chelate 2)	–	11.87	–	–
$-CH_3$ (R' in chelate 1 and 2)	27.82	33.32	–	–
$-C_6H_5$ (R' in chelate 3)	–	–	137.72	–
$-C_6H_4Cl$ (R' in chelate 4)	–	–	–	128.78
Ring phenyl (N1-Phenyl, C-ipso)	148.56	148.34	149.09	148.77
Ring phenyl (C-ortho)	128.8	128.83	128.89	128.94
Ring phenyl (C-meta)	125.43	126.89	126.12	126.39
Ring phenyl (C-para)	121	121.04	121.03	121.09
Thiophenol ring (C-ipso, C–S–Sn)	115.16	115.29	115.44	115.24
Thiophenol ring (C-para)	118.67	119.08	119.63	118.62
Thiophenol ring (C-ortho)	118.14	117.68	118.9	116.68
Thiophenol ring (C-meta)	121	121.04	120.73	120.88
Sn–R (aliphatic)	8.87	7.87	8.78	8.41

Abbreviation: R: Functional group.

The MW analysis conducted in chloroform solution at 45°C demonstrated that these compounds exist as monomers. Spectroscopic analysis revealed that the Schiff bases act as bifunctional tridentate ligands. Analysis of the ^{119}Sn NMR spectra indicated that the Sn atom exhibits pentacoordinate geometry.[35]

3.2. DFT calculations

Using DFT, we analyzed the comparative reactivity patterns of various Sn complexes. The analysis incorporated multiple reactivity descriptors, examining both global parameters (electrophilic and nucleophilic character) and their localized counterparts.

The study included calculations of fundamental electronic properties, such as the highest occupied electron orbital (HOMO) and lowest unoccupied molecular orbital (LUMO) energy levels. These molecular orbital energies were used to derive key chemical descriptors, including the molecule's ability to donate (ionization potential) and accept (electron affinity) electrons, chemical hardness and electronegativity, electrophilic behavior, and electronic chemical potential. These correlations provide insights into the molecular characteristics of the complexes.

3.2.1. Geometrical parameters

The DFT-optimized geometry of the Sn chelates is depicted in Figure 2, and the corresponding bond lengths and bond angles for the Sn complexes are listed in Table 5. In the Sn^{2+} complexes, Mulliken charge analysis was performed for Sn and the coordinating atoms (O, S, nitrogen [N]), as well as the two methyl groups. This analysis indicates that electron transfer from the ligands to Sn is consistent across all chelates, regardless of the substituent. Upon complexation, Sn experiences a loss of approximately 0.7e, resulting in a charge of +1.325 (down from +2). The coordinating atoms, O and N, possess similar Mulliken charges (−0.55 and −0.60, respectively), while S carries a slightly smaller charge (−0.2).

In the optimized structures, the bond distances between Sn and the heteroatoms O and N are 2.1 Å and 2.2 Å, respectively, whereas the Sn–S bond distance is longer, at 2.6 Å. The bond lengths for the two methyl groups covalently bonded to Sn (Sn–C8 and Sn–C8') are shorter, measuring 2.1 Å. Notable differences in coordinating bond angles are observed as a result of steric effects, particularly when substituting methyl groups with chlorophenyl rings. The bond angles between the two methyl groups attached to the Sn ion (C8'–Sn–C) fall within the range of 126° – 127°, while the ∠O–Sn–N angles range from 80° to 81°, and

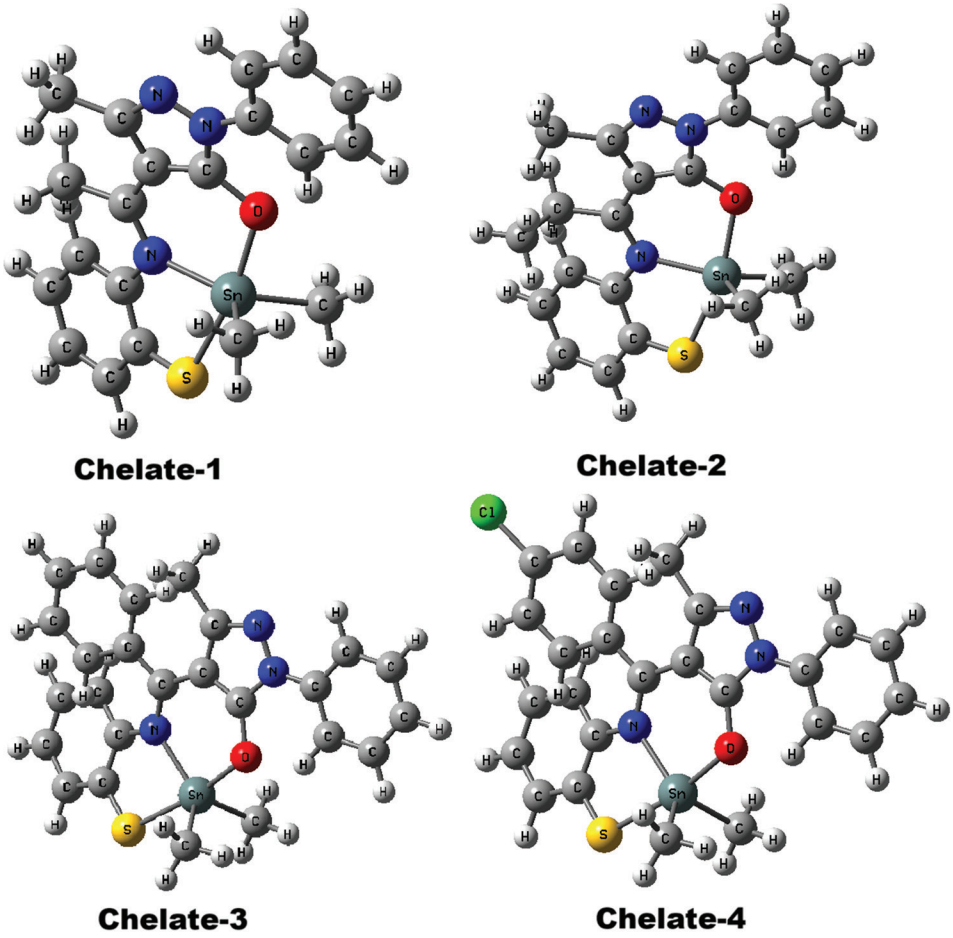

Figure 2. The optimized structure of Sn-complexes calculated using the B3LYP/LanL2DZ method

the ∠N–Sn–S angles are approximately 78°. In addition, a wider and more irregular range (96° – 120°) is observed for bond angles between Sn and the methyl carbon atoms (∠C–Sn–S and ∠C–Sn–C).

As the bulkiness of the substituent increases, a slight decrease in the ∠O–Sn–N angle is observed: from methyl to ethyl, the reduction is 0.36°, from ethyl to phenyl, 0.07°, and from phenyl to chlorophenyl, 0.14°. A similar trend is seen in the ∠N–Sn–S angle (0.27° → 0.20° → 0.12°). Overall, the DFT-optimized structures reveal no significant variations in Mulliken charges or bond lengths across chelates with different substituents, except for differences in bond angles. A separate table (Table 6) presents the computed electronic parameters, including the electron donation and acceptance tendencies (ionization potential and electron affinity), electronic distribution characteristics (electronegativity and chemical hardness), and reactivity indicators (electrophilicity index and chemical potential).

3.2.2. Global reactivity descriptors

Frontier orbital theory explains molecular behavior through two key electronic states: the HOMO and the first empty level above it (LUMO). The energy difference between these frontier orbitals serves as a valuable indicator of the molecule's stability and potential reaction pathways. This energetic separation helps predict how readily the molecule can participate in chemical transformations. A small HOMO-LUMO gap indicates that the molecule requires less energy to excite electrons, suggesting higher reactivity, while a large gap implies greater chemical stability.

The HOMO reflects a molecule's ability to donate electrons, corresponding to ionization potential, while the LUMO reflects its ability to accept electrons, corresponding to electron affinity. Ionization potential represents the energy needed to remove an electron from the molecule, with a high value indicating greater stability and inertness, while lower values suggest increased reactivity. Electron

affinity refers to the energy released when an electron is added to the molecule, and higher values imply a greater tendency to accept electrons.

According to calculations performed using the B3LYP/LanL2DZ method, the predicted HOMO and LUMO values for the Sn chelates are −0.20 eV and −0.08 eV, respectively. From these values, the HOMO-LUMO energy gap (ΔE) is calculated to be 0.12 eV, indicating the molecule's electronic properties. As observed in Figure 3, analysis of the frontier orbital distributions revealed distinct electronic patterns: the highest occupied state showed significant electron density around the S-containing portion of the molecule, whereas the lowest unoccupied state exhibited electron density spread across both the imidazole moiety and S region. We employed Koopman's theorem,[36] which applies to closed-shell systems, to compute global reactivity parameters.

Table 5. Selected molecular parameters and dipole moment (debye) of organotin (IV) complexes

Parameter	Chelate-1	Chelate-2	Chelate-3	Chelate-4
Dipole moment	3.010	2.856	3.440	2.129
Mulliken charge (e)				
Sn	1.326	1.325	1.325	1.325
O	−0.557	−0.555	−0.546	−0.546
N	−0.568	−0.590	−0.584	−0.581
S	−0.192	−0.198	−0.196	−0.193
Bond angle (°)				
O–Sn–N	81.390	81.034	80.969	80.833
N–Sn–S	78.248	77.973	77.772	77.656
S–Sn–C25	120.754	95.626	100.919	101.067
S–Sn–C26	101.030	101.445	96.515	96.654
C25–Sn–C26	126.164	125.688	126.612	126.499
Bond distance (Å)				
O–Sn	2.134	2.135	2.148	2.148
N–Sn	2.185	2.177	2.177	2.180
S–Sn	2.611	2.617	2.612	2.611
Sn–C26	2.118	2.118	2.118	2.117
C25–Sn	2.128	2.128	2.127	2.127

Our findings from these calculations were quantitatively documented in Table 5. The ionization potential of the complexes is 0.20 eV, and the electron affinity (A) is in the range of 0.076 – 0.089 eV. The hardness of the complexes is calculated to be approximately 0.06 eV across all chelates. However, the softness values for the methyl (Chelate-1) and ethyl (Chelate-2) substituents are around 7.8, while for phenyl (Chelate-3) and chlorophenyl (Chelate-4) substituents, they are slightly higher, at 8.4 and 8.6, respectively, indicating increased reactivity in the phenyl-substituted compounds. The electrophilicity index of the complexes is calculated to be 0.001 eV, which is relevant for describing their biological activity. The chemical potential of the complexes is −0.14 eV, a negative value, suggesting that these complexes are chemically stable.

3.3. Docking analysis

We performed molecular docking simulations on the above DFT-optimized structures. The docking analysis utilized cephalosporin and sulfamethoxazole as reference ligands for transpeptidase and dihydropteroate synthase, respectively, to benchmark the binding affinities of the ligands (L-1 to L-4) against selected bacterial target proteins (5TW8, 6NTW, 1AD4, and 5V7A), as shown in Table 7. Molecular docking was conducted using only the ligand moieties of the organotin (IV) complexes, with the

Table 6. Global reactivity descriptors and energies of organotin (IV) complexes on the B3LYP/LanL2DZ basis set

Molecular properties	Expression	Chelate-1	Chelate-2	Chelate-3	Chelate-4
E_{HOMO}, ev	Energy of H_{OMO}	−0.204	−0.203	−0.202	−0.207
E_{LUMO}, ev	Energy of L_{UMO}	−0.076	−0.077	−0.083	−0.090
E_{Gap}, ev	$E_{HOMO}-E_{LUMO}$	0.128	0.127	0.119	0.117
Ionization potential, ev	$-E_{HOMO}$	0.204	0.203	0.202	0.207
Electron affinity, ev	$-E_{LUMO}$	0.076	0.077	0.083	0.090
Chemical hardness (η), ev	$1/2\ (E_{LUMO}-E_{HOMO})$	0.064	0.063	0.059	0.058
Softness, S	$1/2\eta$	7.829	7.883	8.408	8.559
Chemical potential (μ), ev	$1/2\ (E_{LUMO}+E_{HOMO})$	−0.140	−0.140	−0.143	−0.148
Electronegativity (χ), ev	$-1/2\ (E_{LUMO}+E_{HOMO})$	0.140	0.140	0.143	0.148
Electrophilicity index (ω), ev	$\mu^2/2\eta$	0.001	0.001	0.001	0.001
Optimized energy, au	E	−1,027.7	−1,066.9	−1,219.4	−1,233.7

Abbreviations: HOMO: Highest occupied electron orbital; LUMO: Lowest unoccupied molecular orbital.

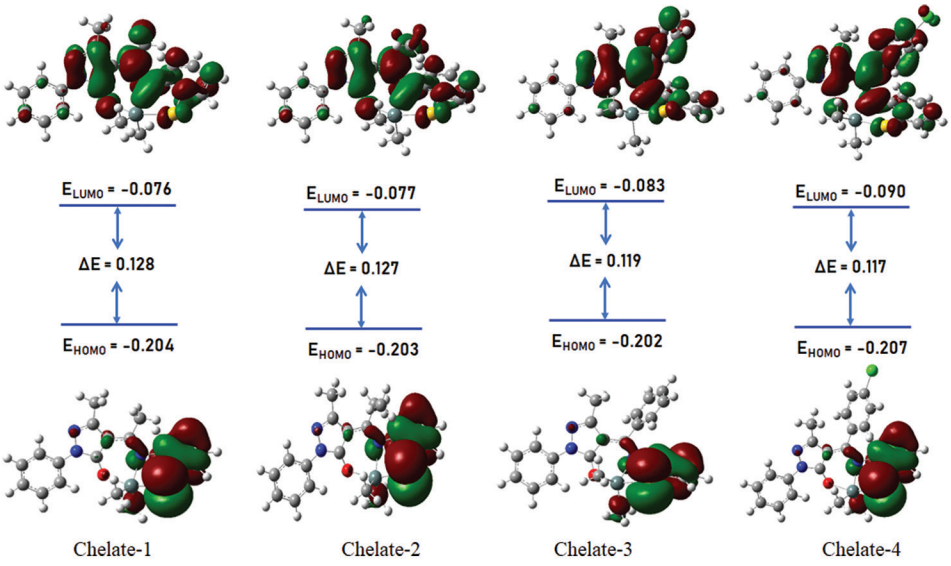

Figure 3. Highest occupied electron orbital plot of Sn-complexes performed by DFT/B3LYP level with LanL2DZ basis set

Sn center deliberately excluded. This decision was made to minimize computational expense and simplify the docking simulations, as the inclusion of a heavy metal such as Sn significantly increases system complexity due to its relativistic effects and lack of consistent parameterization in many docking software packages. Since the Sn atom remains constant across all complexes studied and the primary variations in binding affinities are attributed to the structural differences in the organic ligand frameworks, the docking results are expected to reflect the influence of ligand architecture on biological target affinity, independent of the Sn center.

Figure 4 depicts key residue interactions of target proteins (5TW8, 6NTW, 1AD4, and 5V7A), with test ligands (L-1, L-2, L-3, and L-4). We also considered key residue interactions of Gram-positive (5TW8, 6NTW) and Gram-negative (1AD4, 5V7A) strains with reference ligands for comparison of their corresponding binding abilities. The docking results are categorized into two distinct sections. The first section evaluates the antibacterial activity of the test ligands along with the cephalosporin reference ligand against transpeptidase enzymes. Binding values presented in Table 7 indicate that the binding order for 5TW8 is L-4 > L-3 > L-1 > L-2 > cephalosporin. Among them, ligand L-4 demonstrates the most favorable binding energies, with −8.50 kcal/mol for 5TW8, which is significantly higher than that of the cephalosporin (−5.72 kcal/mol). In 5TW8, cephalosporin interacts with several key residues, including Ser139, Ser262, Arg186, Glu183, Ser75, Ser116, Lys78, and Ala074, highlighting a diverse range of polar and charged contacts. The test ligands also share several of these crucial interactions, notably with Ser262, Ser075, and Ala074 residues. L-1 and L-2 maintain similar interaction profiles, while L-3 and L-4 form additional contacts with Phe241 and Ala182 residues, which likely contribute to their enhanced binding affinity.

In case of 6NTW, the order is L-4 > cephalosporin > L-3 > L-2 > L-1. Among them, ligand L-4 demonstrates the most favorable binding energies, with −9.48 kcal/mol for 6NTW, which is significantly higher than that of the cephalosporin (−7.53 kcal/mol). Here, cephalosporin interacts with a broad set of residues, including Pro501, Ser502, Met500, Glu504, Lys497, Asn426, Tyr507, Ala505, Pro428, and Trp425. L-1 shares four common binding residues with cephalosporin and additionally interacts with Ser526 and Cys528. L-2 displays a similar interaction profile but also engages with Ile506, His509, and Leu431. L-3, which nearly matches cephalosporin in binding strength, interacts with His509, Cys528, Ala505, Ser526, and Leu431, indicating that these residues may play a critical role in stabilizing the ligand-protein complex. L-4 establishes interactions with multiple critical residues, including His509, Tyr507, Ala505, Pro428, Leu431, Cys528, and Trp425, offering both polar and hydrophobic contacts that contribute to stable binding. Notably, specific residues such as Ser262, Ala074, and Ser075 in 5TW8, along with Tyr507, Ala505, Cys528, and Trp425 in 6NTW, are consistently involved in the binding of both cephalosporin and the test ligands, indicating conserved hotspots within the binding pockets of the transpeptidase enzyme.

The second section deals with the interactions of the test ligands along with the sulfamethoxazole reference ligand against dihydropteroate synthase enzymes. Table 7 indicates

Table 7. Comparative binding energies and key residue interactions of test ligands (L-1 to L-4) and control drugs (cephalosporin and sulfamethoxazole) with bacterial target proteins: transpeptidase (5TW8, 6NTW) and dihydropteroate synthase (1AD4, 5V7A)

Ligands	Target protein	Binding energy	Active amino acid and hydrogen bond interaction
Cephalosporin	5TW8	−5.72	Ser 139, Ser 262, Arg 186, Glu 183, Ser 075, Ser 116, Lys 078, Ala 074
L-1	5TW8	−6.77	Ser 262, Ala 074, Ala 182, Ser 075, Ser 262
L-2	5TW8	−6.66	Leu 115, Ala 074, Ser 075, Ser 262
L-3	5TW8	−7.27	Phe 241, Ser 262, Ser 260, Ser 075, Ala 074, Ala 182
L-4	5TW8	−8.50	Ser 075, Ser 139, Ala 074, Ala 182, Phe 241
Cephalosporin	6NTW	−7.53	Pro 501, Ser 502, Met 500, Glu 504, Lys 497, Asn 426, Tyr 507, Ala 505, Pro 428, Trp 425
L-1	6NTW	−6.78	Ser 526, Cys 528, Tyr 507, Pro 428, Trp 425, Ala 505
L-2	6NTW	−6.88	Pro 428, Trp 425, Ile 506, Cys 528, His 509, Leu 431, Ser 526
L-3	6NTW	−7.50	His 509, Cys 528, Ala 505, Ser 526, Leu 431
L-4	6NTW	−9.48	His 509, Tyr 507, Ala 505, Pro 428, Leu 431, Cys 528, Trp 425
Sulfamethoxazole	1AD4	−6.20	Ala 199, Asn 103, Met 128, Asp 84, Arg 239, Phe 172, Asp 167
L-1	1AD4	−6.98	Lys 203, Ala 199 Arg 239, Phe 172, Met 128, Asp 84, Ser 201, His 241, Asn 103
L-2	1AD4	−6.16	Lys 203, Arg 239, Phe 172, Asn 103, Asp 084, Ala 199, Met 128
L-3	1AD4	−6.89	Lys 203, Arg 239, Asp 084, Asn 103, Ser 201, Ala 199, Phe 172, Met 128
L-4	1AD4	−9.00	Phe 172, Asp 167, Met 128, Arg 239, Lys 203, His 055, Ile 009, Val 049
Sulfamethoxazole	5V7A	−6.43	Asn 022, Arg 063, Lys 221, Thr 062, Arg 255, Met 139, Phe 190, Ser 061
L-1	5V7A	−6.67	Asp 096, Lys 221, His 257, Ile 020, Thr 062, Phe 190
L-2	5V7A	−6.79	Arg 063, Pro 064, His 257, Phe 190, Thr 062, Ser 061, Glu 060
L-3	5V7A	−7.48	Arg 063, Thr 062, Phe 190, Lys 221, Arg 255, His 257, Ser 219, Asp 096
L-4	5V7A	−9.10	Glu 060, Ser 061, Met 148, Phe 190, Gly 189, Arg 220, His 257, Ile 020, Thr 062, Arg 063, Arg 255

(Cont'd...)

Table 7. ***(Continued)***

that the order of binding affinity of the ligands against the 1AD4 protein is L-4 > L-1 > L-3 > sulfamethoxazole >L-2. The standard drug sulfamethoxazole showed interactions with the Ala199, Asn103, Met128, Asp84, Arg239, Phe172, and Asp167 residues of 1AD4 protein. L-1 retains most of these interactions and further establishes additional contacts with Lys203, Ser201, and His241, which likely contribute to its enhanced stability within the active site. Similarly, L-3 shares all major binding residues of sulfamethoxazole and also forms supplementary interactions with Lys203 and Ser201. In contrast, L-2, despite sharing several binding residues with the control, shows no significant gain in binding strength. L-4 exhibits a significantly stronger binding affinity (−9.00 kcal/mol) compared to the reference drug (−6.20 kcal/mol). Both the L-4 and sulfamethoxazole share common interactions with Phe172, Asp167, Met128, and Arg239. In addition to these, L-4 establishes interactions with Lys203, His055, Ile009, and Val049, expanding its binding network and likely contributing to its enhanced stability and inhibitory potential.

In the case of the 5V7A protein, the binding affinity follows the order: L-4 > L-3 > L-2 > L-1 > sulfamethoxazole. Sulfamethoxazole forms interactions with several key residues of the 5V7A protein, including Asn022, Arg063, Lys221, Thr062, Arg255, Met139, Phe190, and Ser061, indicating its engagement with both polar and hydrophobic sites. L-1 retains interactions with Lys221, Thr062, and Phe190, which are also involved in sulfamethoxazole binding, and introduces additional contacts with Asp096, His257, and Ile020. L-2 also shares common residues, such as Arg063, Thr062, Phe190, and Ser061, while forming new interactions with Pro064, His257, and Glu060, contributing to a more diverse binding profile. Notably, both L-3 and L-4 exhibit a shared interaction network that significantly overlaps with that of sulfamethoxazole, particularly at key residues such as Arg063, Thr062, Phe190, and Arg255. In addition to these common interactions, L-3 establishes further contacts with His257, Ser219, and Asp096, enhancing its binding profile. Meanwhile, L-4 engages with several new residues,

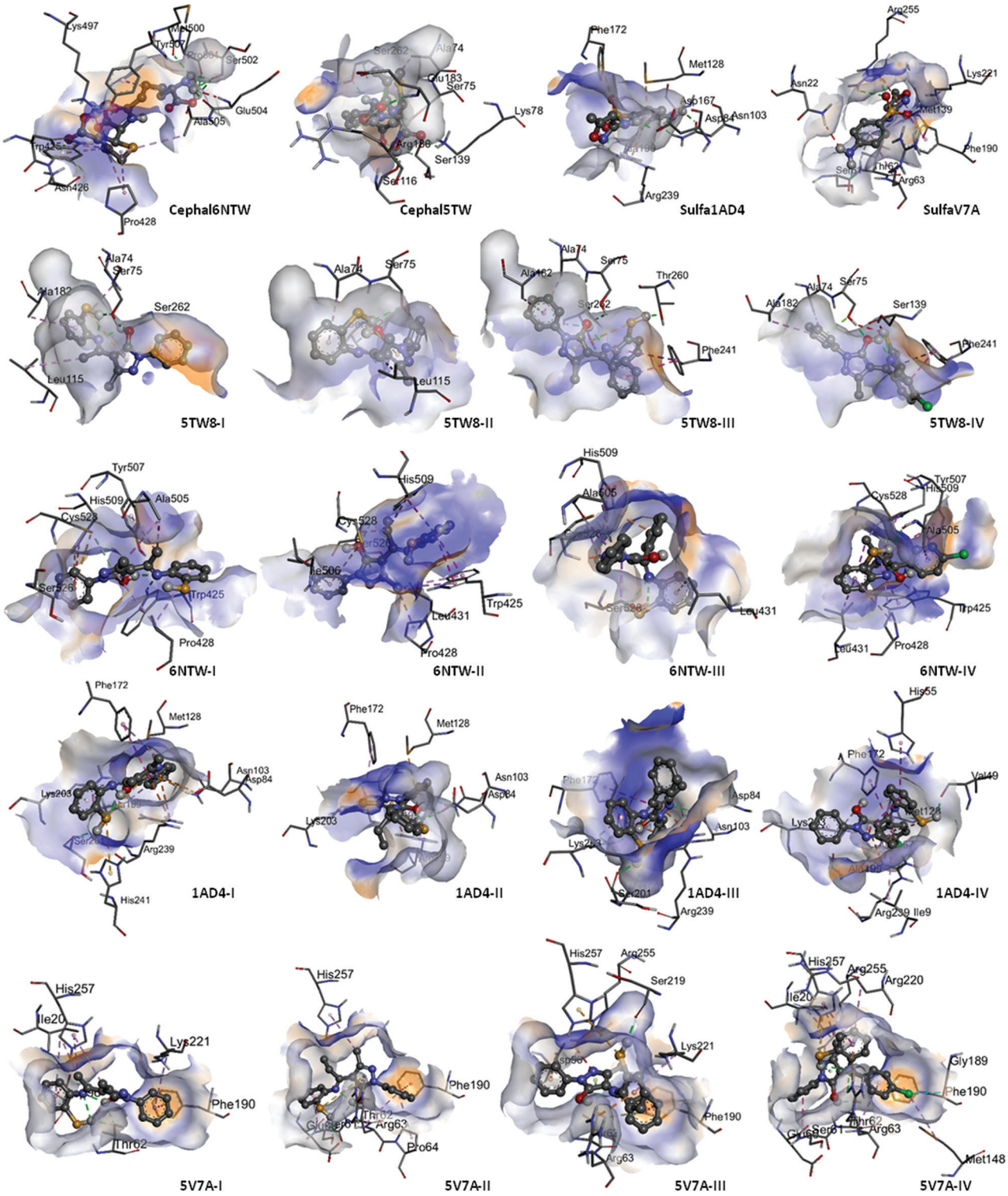

Figure 4. 3D representations of ligand binding within the active sites of transpeptidase (protein database IDs: 5TW8 and 6NTW) and dihydropteroate synthase (protein database IDs: 1AD4 and 5V7A). Ligands are depicted in ball-and-stick style with element-specific colors, while interacting protein residues are shown as sticks colored by residue type.
Notes: Ligands I-IV correspond to ligands L1-L4, respectively. "Cephal" refers to cephalosporin, and "Sulfa" refers to sulfamethoxazole.

including Glu060, Met148, Gly189, Arg220, His257, and Ile020, thereby considerably expanding its interaction network. These additional contacts are likely to strengthen binding affinity through a combination of hydrogen bonding, electrostatic interactions, and hydrophobic effects. Overall, these findings suggest that ligand L-4, followed by L-3, holds significant potential as a promising antibacterial agent targeting dihydropteroate synthase and transpeptidase enzymes.

3.4. Prediction of drug-likeness of ligands by the SwissADME tool

The SwissADME tool (https://www.swissadme.ch/) was employed to evaluate the *in silico* pharmacokinetic properties of ligands L-1 to L-4, with each molecule converted into its canonical Simplified Molecular Input Line Entry System format. The drug-likeness of these ligands, referring to their potential suitability as orally active drugs, was assessed using Lipinski's rule of five, a widely accepted guideline for predicting oral bioavailability based on key physicochemical properties.[37] The physicochemical properties relevant to ADME profiling include several key parameters (Table 8). An ideal drug candidate typically has a MW of 500 g/mol or less. The log *p*-value, representing lipophilicity, should not exceed 5, as higher values may lead to poor aqueous solubility. The topological polar surface area (TPSA) should be 140 Å^2 or less for adequate absorption, with values below 90 Å^2 being particularly favorable for blood-brain barrier (BBB) penetration. Furthermore, compounds should possess no more than five hydrogen bond donors and 10 hydrogen bond acceptors to ensure good membrane permeability. The number of rotatable bonds should ideally be 10 or fewer, which contributes to conformational flexibility and oral bioavailability. Finally, zero to one violation of Lipinski's rules is generally acceptable for a compound to be considered drug-like.

As shown in Table 8, the four ligands exhibit distinct drug-likeness profiles, determined by their compliance with Lipinski's rule of five and core physicochemical properties. The first ligand, L-1, demonstrates excellent drug-like properties, with a MW of 325.43, a log P of 4.3, a TPSA of 88.88 Å^2, four rotatable bonds, and two hydrogen bond donors and acceptors, resulting in zero Lipinski violations. The L-2 also complies fully with Lipinski's criteria, showing a slightly higher log P of 4.83 and MW of 339.45, while remaining within acceptable limits for oral bioavailability. In contrast, L-3 exceeds the recommended log P threshold, with a value of 5.59, resulting in one Lipinski violation. While other parameters, such as MW of 387.50 g/mol, TPSA of 88.88 Å^2, and hydrogen bonding characteristics, are within desirable ranges, the elevated lipophilicity may negatively affect its aqueous solubility and absorption. The fourth ligand, L-4, has a MW of 421.94 g/mol and a high log P of 6.22, leading to one Lipinski violation as well. The inclusion of a chlorine atom likely contributes to this increased lipophilicity, which may impair its solubility and pharmacokinetic profile despite acceptable TPSA and

Table 8. Physicochemical, pharmacokinetic, and drug-likeness properties of ligands (L-1 to L-4)

Ligand	L-1	L-2	L-3	L-4
Formula	$C_{18}H_{19}N_3OS$	$C_{19}H_{21}N_3OS$	$C_{23}H_{21}N_3OS$	$C_{23}H_{20}ClN_3OS$
Molecular weight (g/mol)	325.43	339.45	387.5	421.94
Log *p*-value	4.3	4.83	5.59	6.22
Topological polar surface area (Å^2)	88.88	88.88	88.88	88.88
Rotatable bonds	4	5	5	5
Hydrogen bond donors/acceptors	2/2	2/2	2/2	2/2
Lipinski violations	0	0	1	1
Gastrointestinal absorption	High	High	High	High
Blood-brain barrier permeant	No	No	No	No
P-glycoprotein substrate	No	No	Yes	Yes
CYP1A2 inhibitor	Yes	Yes	No	No
CYP2C19 inhibitor	Yes	Yes	Yes	Yes
CYP2C9 inhibitor	Yes	Yes	Yes	Yes
CYP2D6 inhibitor	Yes	Yes	Yes	Yes
CYP3A4 inhibitor	Yes	Yes	Yes	Yes
Log K*p* skin permeation (cm/s)	−5.23	−4.94	−4.69	−4.69

Abbreviation: CYP: Cytochrome P450 enzyme.

hydrogen bonding features. Overall, ligands 1 and 2 appear highly favorable for further development, while ligands 3 and 4, though structurally promising, may require additional formulation or optimization efforts due to their higher lipophilicity.

In drug discovery, several ADME-related parameters are crucial for assessing a compound's pharmacokinetic profile. Gastrointestinal absorption reflects the ability of a drug to be absorbed through the digestive tract, which is crucial in achieving effective oral bioavailability. BBB permeability determines whether a compound can cross into the central nervous system; while this is desirable for central nervous system (CNS)-targeted drugs, it may be avoided in non-CNS drugs to reduce neurological side effects. The status of a compound as a P-glycoprotein (P-gp) substrate influences its distribution and bioavailability, as P-gp actively transports substances out of cells, potentially lowering intracellular drug concentrations.

According to the *in-silico* ADME analysis, all four ligands presented in Table 8 exhibit high gastrointestinal absorption, implying good oral bioavailability potential. However, none of the ligands are predicted to be BBB permeant, suggesting limited potential for central nervous system activity, which may be advantageous in reducing neurological side effects for non-CNS targets. Notably, the L-1 and L-2 are not substrates of P-gp, implying lower chances of efflux-related bioavailability reduction. In contrast, L-3 and L-4 are identified as P-gp substrates, which may lead to reduced intracellular concentrations due to active efflux, particularly in the intestine or BBB regions.

The inhibition of cytochrome P450 (CYP) enzymes, such as CYP1A2, CYP2C19, CYP2C9, CYP2D6, and CYP3A4, can lead to significant drug–drug interactions (DDIs) by affecting the metabolism of co-administered therapies. Notably, CYP3A4 metabolizes a large proportion of clinically used drugs. All four ligands are predicted to inhibit multiple major cytochrome P450 enzymes, namely CYP2C19, CYP2C9, CYP2D6, and CYP3A4, while the first two ligands additionally show inhibition of CYP1A2 (Table 8). Such broad-spectrum inhibition suggests a high potential for DDIs, which could complicate co-administration with other medications metabolized by these enzymes. Skin permeability, measured as log K_p, estimates a compound's ability to penetrate the skin; higher negative values suggest lower transdermal absorption, which is important for evaluating the potential of dermal exposure or suitability for topical drug delivery. As shown in Table 8, the skin permeability values (log K_p) progressively increase from ligand L-1 to L-4 (from −5.23 to −4.46 cm/s), indicating a gradual increase in their potential to permeate the skin across the series. Despite this trend, all values remain within the range, indicating moderate to low skin permeability. Overall, while the compounds show strong oral absorption profiles, caution is warranted due to their CYP inhibition profiles and P-gp substrate status, particularly for L-3 and L-4. These factors may influence both efficacy and safety during drug development, requiring further ADME profiling and possible structural refinement to mitigate risks.

In several cases, increased steric hindrance may prevent hydrolysis or metabolic degradation, allowing the complex to reach the target intact and potentially increasing its selectivity or prolonging its activity.[38] Bulkier groups generally increase lipophilicity, which may enhance membrane permeability, potentially increasing bioactivity in lipophilic environments (e.g., tumor cell membranes). Steric hindrance around the Sn (IV) center often increases kinetic stability by physically blocking access to reactive sites. This can protect against ligand exchange, hydrolysis, or oxidation, which is especially important in physiological environments (aqueous, neutral pH).[39] Moreover, Schiff base-derived diorganotin (IV) complexes with bulky substituents (e.g., Ph_2SnL vs. Me_2SnL) exhibited a greater antimalarial and antioxidant activity.[40]

4. Conclusion

In the present work, sterically hindered 4-(2'mercapto-phenyl-iminoalkyl/aroyl)-2,4-dihydro-5-methyl-2-phenyl-3H-pyrazol-3-ones ligands were employed for the synthesis of organotin complexes under the specified reaction conditions. Molecular docking studies revealed the extensive interactions of ligands with key active-site residues of proteins. These findings suggest that L-4 possesses strong potential as a broad-spectrum antibacterial agent. In contrast, ligands L-1 and L-3 showed moderate binding affinities, with occasional performance comparable to the reference ligands, while L-2 consistently exhibited the weakest binding across all targets.

DFT calculations suggest that all four chelates display similar electronic properties with only slight variations. Among them, Chelate-4 is the most reactive, characterized by the smallest energy gap, highest electron affinity, and greatest softness, indicating enhanced electron-accepting ability and chemical reactivity. In contrast, Chelate-1 shows the greatest stability with the widest energy gap. These subtle electronic differences suggest that while the chelates share similar molecular frameworks, variations in their reactivity could influence their interactions with biological targets. Although both L-3 and L-4 possess

aromatic rings, L-4 exhibits slightly superior electronic characteristics across all molecular descriptors, such as a lower energy gap, higher softness, and greater electron affinity. These properties render L-4 more reactive and better equipped for strong and flexible interactions within the protein binding pocket, which is consistent with its enhanced binding affinities observed in docking studies.

From a drug-likeness and pharmacokinetic context, L-1 and L-2 emerged as the most promising candidates. Both fully adhered to Lipinski's rule of five, with MWs under 340 g/mol, optimal log *p*-values (4.30 and 4.83, respectively), suitable TPSA of <140 Å^2, and no Lipinski violations, suggesting good oral bioavailability. On the other hand, L-3 and L-4 each had one Lipinski violation due to higher log *p*-values (5.59 and 6.22, respectively), indicating increased lipophilicity, which may affect solubility and absorption. For L-4, the presence of a chlorine atom likely contributes to this elevated lipophilicity.

Acknowledgments

None.

Funding

None.

Conflict of interest

The authors declare that they have no competing interests.

Author contributions

Conceptualization: Shama Chauhan, Rupa Madyal
Data curation: Harlal Singh, Venkatanarayana Pappula
Formal analysis: Rupa Madyal, Harlal Singh, Venkatanarayana Pappula
Investigation: Rupa Madyal, Shama Chauhan
Methodology: Rupa Madyal, Harlal Singh, Venkatanarayana Pappula
Supervision: Shama Chauhan, Rupa Madyal
Validation: Harlal Singh, Venkatanarayana Pappula
Writing–original draft: Shama Chauhan, Harlal Singh
Writing–review & editing: Rupa Madyal, Venkatanarayana Pappula

Ethics approval and consent to participate

Not applicable.

Consent for publication

Not applicable.

Availability of data

Data will be made available on request.

References

1. Hadjikakou SK, Hadjiliadis N. Antiproliferative and anti-tumor activity of organotin compounds. *Coord Chem Rev.* 2009;253(1-2):235-49.

   doi: 10.1016/j.ccr.2008.09.017

2. Nath M, Sharma CL, Sharma N. Dibutyltin(IV) complexes of schiff bases derived from aminoacids. *Synth React Inorg Met Org Chem.* 1991;21(5):807-24.

   doi: 10.1080/15533179108016844

3. Bhambhani S, Saxena S, Rai AK. New dibutylgermanium (IV) complexes of sterically demanding 4-(2'-mercapto phenyl iminoalkyl/aroyl)-2, 4-dihydro-5-methyl-2-phenyl-3h-pyrazol-3-ones: Preparation and structural elucidation. *Main Group Met Chem*. 1998;21(12):747-750.

   doi: 10.1515/MGMC.1998.21.12.747

4. Nath M, Yadav R, Eng G, Nguyen TT, Kumar A. Characteristic spectral studies, and antimicrobial and anti-inflammatory activities of diorganotin (IV) derivatives of dipeptides. *J Organomet Chem.* 1999;577(1):1-8.

   doi: 10.1016/S0022-328X(98)01017-1

5. Bhambhani S, Saxena S, Rai AK. Synthetic and structural aspects of certain diorganosilicon (IV) chelates derived from sterically demanding 4-(2'-mercapto phenyl imino alkyl/aryl)-2,4-dihydro-5-methyl-2-phenyl-2H-pyrazol-3-ones. *Phosphorus Sulfur Silicon Relat Elem.* 2000;157(1):29-41.

   doi: 10.1080/10426500008040510

6. Sharma J, Singh YP, Rai AK. Synthesis, characterization and structural elucidation of monoorganodi (chloro) Sn(IV) complexes of heterocyclic dithiocarbamates. *Main Group Met Chem.* 2000;23(5):317-20.

   doi: 10.1515/MGMC.2000.23.5.317

7. Sharma J, Singh Y, Bohra R, Rai AK. Synthesis and spectral studies of diorganotin heterocyclic dithiocarbamate complexes: The crystal structure of $(CH_3)_2Sn[(S_2CNCH_2CH_2CH_2CH_2CH_2]_2$. *Polyhedron.* 1996;15(7):1097-1102.

   doi: 10.1016/0277-5387(95)00341-X

8. Singh HL, Singh J. Synthesis, spectroscopic, molecular structure, and antibacterial studies of dibutyltin (IV) Schiff base complexes derived from phenylalanine, isoleucine, and glycine. *Bioinorg Chem Appl.* 2014;2014(1):716578.

   doi: 10.1155/2014/716578

9. Zhang Q, Zhang M, Wang H, *et al*. A series of two-photon absorption organotin (IV) cyano carboxylate derivatives for targeting nuclear and visualization of anticancer activities. *J Inorg Biochem.* 2019;192:1-6.

   doi: 10.1016/j.jinorgbio.2018.12.009

10. Adeyemi JO, Onwudiwe DC. Organotin (IV)

dithiocarbamate complexes: Chemistry and biological activity. *Molecules*. 2018;23(10):2571.

doi: 10.3390/molecules23102571

11. Singh HL, Dhingra N, Bhanuka S. Synthesis, spectral, antibacterial and QSAR studies of tin and silicon complexes with Schiff base of amino acids. *J Mol Struct.* 2023;1287:135670.

doi: 10.1016/j.molstruc.2023.135670

12. Shah FA, Sirajuddin M, Ali S, Abbas SM, Tahir MN, Rizzoli C. Synthesis, spectroscopic characterization, X-ray structure and biological screenings of organotin (IV) 3-[(3, 5-dichlorophenylamido)] propanoates. *Inorg Chim Acta.* 2013;400:159-168.

doi: 10.1016/j.ica.2013.12.022

13. Liu J, Lin Y, Liu M, *et al*. Synthesis, structural characterization and cytotoxic activity of triorganotin 5-(salicylideneamino) salicylates. *Appl Organomet Chem.* 2019;33(3):e4715.

doi: 10.1002/aoc.4715

14. Latha A, Elangovan N, Manoj KP, *et al*. Synthesis, single crystal (XRD), spectral characterization, computational (DFT), quantum chemical modelling and anticancer activity of di (p-bromobenzyl)(dibromo)(1, 10-phenanthroline) tin(IV) complex. *J Indian Chem Soc.* 2022;99(10):100714.

doi: 10.1016/j.jics.2022.100714

15. Bhaskar C, Elangovan N, Sowrirajan S, *et al*. Synthesis, XRD, Hirshfeld surface analysis, DFT studies, cytotoxicity and anticancer activity of di(m-chlorobenzyl)(dichloro) (4,7-diphenyl-1,10-phenanthroline) tin(IV) complex. *J Mol Struct.* 2022;1267:133542.

doi: 10.1016/j.molstruc.2022.133542

16. Sharma A, Dhingra N, Singh HL, Khaturia S, Bhardawaj U. New complexes of organotin(IV) and organosilicon(IV) with 2-{(3,4-dimethoxybenzylidene) amino}-benzenethiol: Synthesis, spectral, theoretical, antibacterial, docking studies. *J Mol Struct.* 2022;1261:132812.

doi: 10.1016/j.molstruc.2022.132812

17. Pooyan M, Shariatinia Z, Mohammadpanah F, *et al*. *In vitro* cytotoxicity evaluation of organotin(IV) complexes derived from bisphosphoramide ligand: DNA binding and molecular docking studies. *J Mol Liq.* 2023;391:123442.

doi: 10.1016/j.molliq.2023.123442

18. Mansour MS, Ibrahium AT, El-Sherif AA, Mahmoud WH. Organotin(IV) complexes: Synthesis, characterization, DFT, and molecular docking studies unveiling their potential biomedical uses. *Appl Organomet Chem.* 2024;38(11):e7656.

doi: 10.1002/aoc.7656

19. Meng XY, Zhang HX, Mezei M, Cui M. Molecular docking: A powerful approach for structure-based drug discovery. *Curr Comput Aided Drug Des.* 2011;7(2):146-157.

doi: 10.2174/157340911795677602

20. Palafox MA, Tardajos G, Guerrero-Martínez A, *et al*. FT-IR, FT-Raman spectra, density functional computations of the vibrational spectra and molecular geometry of biomolecule 5-aminouracil. *Chem Phys.* 2007;340(1-3):17-31.

doi: 10.1016/j.chemphys.2006.11.020

21. Khan MA, Kesharwani MK, Bandyopadhyay T, Ganguly B. Remarkable effect of hydroxylamine anion towards the solvolysis of sarin: A DFT study. *J Mol Struct Theochem.* 2010;944(1-3):132-136.

doi: 10.1016/j.theochem.2009.10.003

22. Vogel AI. *A Textbook of Quantitative Inorganic Analysis*. 3rd ed. London, UK: The English Language Book Society and Longman; 1961.

23. Frisch MJ, Trucks GW, Schlegel HB, *et al*. Gaussian 03, Revision 03. Wallingford CT: Gaussian, Inc.; 2004.

24. Hampele IC, D'Arcy A, Dale GE, *et al*. Structure and function of the dihydropteroate synthase from *Staphylococcus aureus*. *J Mol Biol*. 1997;268(1):21-30.

doi: 10.1006/jmbi.1997.0944

25. Dennis ML, Lee MD, Harjani JR, *et al*. 8-mercaptoguanine derivatives as inhibitors of dihydropteroate synthase. *Chem Eur J.* 2018;24(8):1922-1930.

doi: 10.1002/chem.201704730

26. Alexander JA, Chatterjee SS, Hamilton SM, Eltis LD, Chambers HF, Strynadka NC. Structural and kinetic analyses of penicillin-binding protein 4 (PBP4)-mediated antibiotic resistance in *Staphylococcus aureus*. *J Biol Chem.* 2018;293(51):19854-19865.

doi: 10.1074/jbc.RA118.004952

27. Caveney NA, Caballero G, Voedts H, *et al*. Structural insight into YcbB-mediated beta-lactam resistance in *Escherichia coli*. *Nat Commun*. 2019;10(1):1849.

doi: 10.1038/s41467-019-09507-0

28. Saqallah FG, Hamed WM, Talib WH, Dianita R, Wahab HA. Antimicrobial activity and molecular docking screening of bioactive components of *Antirrhinum majus* (snapdragon) aerial parts. *Heliyon*. 2022;8(8):e10391.

doi: 10.1016/j.heliyon.2022.e10391

29. Cochrane SA, Lohans CT. Breaking down the cell wall: Strategies for antibiotic discovery targeting bacterial transpeptidases. *Eur J Med Chem*. 2020;194:112262.

doi: 10.1016/j.ejmech.2020.112262

30. Lima LM, Da Silva BN, Barbosa G, Barreiro EJ. β-lactam antibiotics: An overview from a medicinal chemistry perspective. *Eur J Med Chem*. 2020;208:112829.

doi: 10.1016/j.ejmech.2020.112829

31. Griffith EC, Wallace MJ, Wu Y, *et al*. The structural and

functional basis for recurring sulfa drug resistance mutations in *Staphylococcus aureus* dihydropteroate synthase. *Front Microbiol*. 2018;9:1369.

doi: 10.3389/fmicb.2018.01369

32. Capasso C, Supuran CT. Dihydropteroate synthase (sulfonamides) and dihydrofolate reductase inhibitors. In: *Bacterial Resistance to Antibiotics-From Molecules to Man*. New Jersey: John Wiley and Sons; 2019. p. 163-172.

doi: 10.1002/978111959352

33. Silverstein RM, Webster FX, Kiemle DJ. *Spectrometric Identification of Organic Compounds*. 7th ed. Wiley: New York; 2005. p. 233.

34. Gielen M. An overview of forty years organotin chemistry developed at the Free Universities of Brussels ULB and VUB. *J Braz Chem Soc*. 2003;14:870-877.

doi: 10.1590/S0103-50532003000500021

35. Lyčka A, Holeček J, Sebald A, Tkáč I. Multinuclear NMR study of some diorgano (chloro) tin (IV) oxinates and thiooxinates. *J Organomet Chem*. 1991;409(3):331-9.

doi: 10.1016/0022-328X(91)80019-G

36. Koopmans T. Ordering of wave functions and Eigenenergies to the individual electrons of an atom. *Physica*. 1933;1: 104-113.

37. Lipinski CA, Lombardo F, Dominy BW, Feeney PJ. Experimental and computational approaches to estimate solubility and permeability in drug discovery and development settings. *Adv Drug Deliv Rev*. 1997;23(1-3): 3-25.

doi: 10.1016/S0169-409X(96)00423-1

38. Abd-Aziz NA, Awang N, Chan KM, Kamaludin NF, Mohamad AN. Organotin (IV) dithiocarbamate compounds as anticancer agents: A review of syntheses and cytotoxicity studies. *Molecules*. 2023;28(15):5841.

doi: 10.3390/molecules28155841

39. Devi J, Taxak B, Kumar B, Rani S. Synthesis, characterization and bioactivity of diorganotin (IV) Schiff base complexes as potential antimalarial and antioxidant agents: Insights through cytotoxicity and molecular docking studies. *Dalton Trans*. 2025;54(18):7167-7178.

doi: 10.1039/D5DT00274E

40. Caruso F, Di-Nicola C, Hanna JV, *et al*. Novel bis (β-diketonato) diorganotin (IV) derivatives containing bulky 4-acyl-5-pyrazolonato ligands: Influence of the steric hindrance of the acyl moiety on the solid-state structures of tin complexes and their behaviour in solution. *Inorg Chim Acta*. 2011;367(1):73-84.

doi: 10.1016/j.ica.2010.12.008